

Mixed quantum/classical simulation of the photolysis of HCl on MgO(001)

M. Hintenender and F. Reberstrost

Max-Planck-Institut für Quantenoptik, D-85740 Garching, Germany

R. Kosloff

*Department of Physical Chemistry and The Fritz Haber Research Center of Molecular Dynamics,
The Hebrew University, Jerusalem 91904, Israel*

R. B. Gerber

*Department of Physical Chemistry and The Fritz Haber Research Center of Molecular Dynamics,
The Hebrew University, Jerusalem 91904, Israel and Department of Chemistry, University of California,
Irvine, California 92717*

(Received 23 July 1996; accepted 5 September 1996)

Quantum and mixed quantum/classical calculations of the photolysis of a HCl adsorbate on a MgO surface are reported. In the quantum calculation of the hydrogen dynamics (with rigid surface and chlorine atoms) a strong oscillatory structure is found in the angular distribution of the photofragmented hydrogen as well as in the absorption spectrum. These resonances are caused by temporary trapping of the hydrogen atom between the chlorine atom and the surface and reflect the initial perpendicular adsorption geometry. Corrugation of the surface potential leads to a significant modification of these interference patterns, which exist even for a flat surface. Within a mixed quantum/classical time-dependent self-consistent field (Q/C TDSCF) propagation the influence of surface degrees of freedom on the interference patterns is investigated. The thermal motion of the surface and inelastic collisions of the hydrogen atom with the surface and the chlorine atom washes out most of the oscillatory structure. In the fully angular and energy resolved spectra nevertheless clearly distinguishable peaks are seen. They can be used in practice to extract information about adsorption geometry and surface potential parameters. © 1996 American Institute of Physics. [S0021-9606(96)01646-7]

I. INTRODUCTION

There has been considerable progress in the theoretical modeling of the photodissociation dynamics of small adsorbate molecules on ionic surfaces in the last years. The large number of degrees of freedom made the studies focus predominantly on two situations. One is to use classical molecular dynamics,¹⁻⁴ which can be done with relative ease also in systems with a large number of coordinates. On the other hand, quantum calculations for the photofragments must rely on more stringent dynamical approximations like the one of a rigid surface.⁵⁻⁷ In this study we combine both methods in a mixed quantum/classical time-dependent self-consistent field (Q/C TDSCF) approach. Thereby we get a description of the effects caused by the interplay of the many degrees of freedom of the surface and some specific quantum effects due to the hydrogen dynamics. As example, one of the most interesting questions in this context is, to which extent quantum interference patterns in the spectra are destroyed by inelastic collisions and the thermal motion of the surface.

Other techniques for the simultaneous description of quantum effects and lattice vibrations in related systems were developed for surface scattering⁸ and UV induced desorption.⁹ In these cases the TDSCF separation is also used, but the surface motion is modeled by taking thermal averages over phonon states.

The Q/C TDSCF method does not account for the quantum nature of lattice vibrations, which we expect to be of minor importance at the relevant energies of several eV in

our system. On the other hand the method provides much flexibility to include a large number of surface modes or other classically behaving particles. This is exploited in the present study. In further applications it will be straightforward to extend the model to even more complex situations, as, e.g., the interaction with other, nondissociating coadsorbates. In other contexts the Q/C TDSCF method was used in many dynamical calculations. Among them are reactive scattering¹⁰ or photodissociation in rare gas matrices.^{11,12}

Here we investigate the photodissociation of a single HCl molecule adsorbed on the (001) surface of a MgO crystal. The geometry of this system is believed to be such that the hydrogen atom points initially toward the surface.¹³ By photoexcitation of HCl to the dissociative electronic ¹Π state, the photofragments gain an excess energy of several eV. As a consequence of the initial orientation of the HCl adsorbate, the hydrogen is first accelerated towards the MgO crystal and then backscattered from the surface ions. In this study we consider the resulting energy and angular distributions of the photofragments within the Q/C TDSCF approach and discuss their relation to the initial adsorbate geometry and the surface potential.^{14,15}

II. THE HCl/MgO SYSTEM

A. Potentials and geometry

For the geometry of the system and the potentials we refer to our earlier work on the classical description of the system.⁴ According to the results of a periodic Hartree-Fock

TABLE I. The parameters for the hydrogen potential $V_{\text{H}}(r, \vartheta)$ in the ground state used in the calculation of $\psi(0)$ and the pairwise additive potentials after photoexcitation. The initial distance of the chlorine above the O^{2-} ion of the surface is 5.7 a.u. All values are given in atomic units, ϑ in radians.

$V_{\text{H}}(r, \vartheta) = V_{\text{HCl}}(r) + 1.372 \times 10^{-3} \times \vartheta^2$			
$V_{\text{XY}}(r) = C \left[\left(\frac{\sigma}{r-r_0} \right)^{12} - \left(\frac{\sigma}{r-r_0} \right)^6 \right]$			
H-Cl ($^1\Sigma$):	$C=0.155$	$\sigma=6.5$	$r_0=-3.26$
H-Mg $^{2+}$:	$C=1.30 \times 10^{-3}$	$\sigma=11.2$	$r_0=-5.84$
H-O $^{2-}$:	$C=1.30 \times 10^{-3}$	$\sigma=12.4$	$r_0=-6.48$
Cl-Mg $^{2+}$:	$C=1.525 \times 10^{-5}$	$\sigma=8.963$	$r_0=0$
Cl-O $^{2-}$:	$C=1.767 \times 10^{-3}$	$\sigma=6.132$	$r_0=0$
$V_{\text{HCl}}^{1\Pi}(r) = C e^{-\alpha r}$			
H-Cl ($^1\Pi$):	$C=7.967$	$\alpha=1.733$	
$V_{\text{MgO}}(r) = D \{1 - \exp[-\beta(r-r_0)]\}^2$			
Mg $^{2+}$ -O $^{2-}$:	$D=0.11$	$\beta=0.64$	$r_0=3.70$

calculation with Colle–Salvetti correlation corrected energies,¹³ HCl adsorbs perpendicular to the surface with the hydrogen atom pointing down to one of the oxygen ions of the surface. The equilibrium distance of the adsorbate is somewhat closer to the surface than it was assumed in Ref. 4. The qualitative findings of Ref. 4 are however not affected by this change. Table I summarizes the parameters used in the present study.

In brief, pairwise additive potentials are used for the interactions between the atoms and ions. The MgO crystal is represented by an $8 \times 8 \times 8$ cluster of ions. The Coulomb interaction between the crystal ions is replaced by an effective nearest-neighbor potential, which is adjusted to the MgO phonon frequencies. The interaction of the hydrogen atom with the oscillating ions models the effect of surface phonons.

In the initial state, prior to photodissociation, the weak binding of HCl to the surface results in a large bending motion of the adsorbate due to the zero-point energy. This corresponds to a broad initial wave function for the spatial degrees of freedom of the hydrogen atom (Fig. 1). As discussed

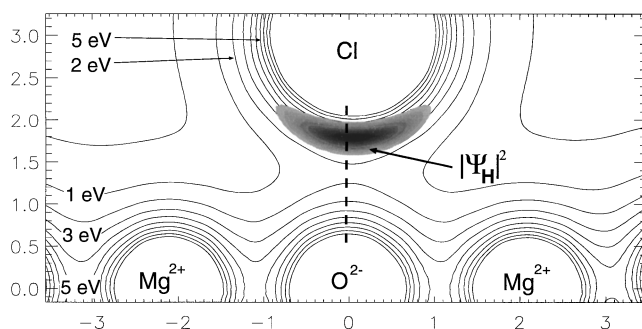


FIG. 1. The zero-point motion of the weakly bound adsorbate leads to a broad distribution of the hydrogen wave packet $|\psi_{\text{H}}|^2$ before photoexcitation. The contour lines show the repulsive potential acting on the hydrogen atom after photoexcitation. The spatial coordinates are in angstrom and the dashed line indicates the cut of Fig. 4.

in detail in Ref. 4 this quantum effect is essential for the dynamics and was therefore modeled already in the classical simulations.

B. Excitation and excited states dynamics

The photoexcitation of the HCl adsorbate is modeled by a Franck–Condon transition to the $^1\Pi$ excited state. At the instant of excitation the ground state wave function $\psi(x, z)$ of the hydrogen atom is transferred to the repulsive $^1\Pi$ potential surface (Fig. 1) and the evolution of the dissociating system is followed by solving the time-dependent Schrödinger equation. In the gas phase the photodissociation of HCl is known to occur by initial excitation to this $A^1\Pi$ state. Only at large distances of the photofragments there is spin–orbit coupling to the $a^3\Pi$ and $1^3\Pi$ triplet states.¹⁶ In this region the potential surfaces are similar and such nonadiabatic transitions have only a minor effect on the dynamics. Here we assume that the system propagates on the $^1\Pi$ state only.

Results of two types of calculations will be shown. First we consider an exact quantum propagation of a hydrogen wave function $\psi(x, z, t)$ in a potential of rigid surface and chlorine atoms. Second we perform a Q/C TDSCF propagation, in which inelastic collisions of the hydrogen atom with the surface and the chlorine atom are allowed. The classical motion of the chlorine atom and the crystal ions due to recoil and thermal motion is included in this calculation. In both cases the motion of the hydrogen atom is restricted to a plane perpendicular to the surface, i.e., described by a two-dimensional wave function $\psi(x, z, t)$ to reduce the numerical effort. In addition, three spatial coordinates for each of the crystal ions and the chlorine atom are propagated by the classical part of the Q/C TDSCF formalism.

From our classical dynamics study⁴ we know that out-of-plane scattering of the hydrogen atom is only important for the higher excitation energies much above the photodissociation threshold. Assuming in-plane scattering the two-dimensional propagation gives correct results for angular resolved spectra in the (x, z) -plane. However, angular independent observables, like the absorption spectrum, are affected by this approximation. The surface normal orientation of the adsorbate favors the trapping of the hydrogen atom discussed later. In the two-dimensional description the relative probability for close to normal configurations is overestimated compared to the three-dimensional case, where non-normal orientations are more likely.

The thermal motion of the surface is taken into account by averaging several Q/C TDSCF runs with different initial configurations of the crystal ions. These configurations are obtained as “snapshots” of a long-time classical propagation of the MgO cluster without adsorbate at a surface temperature $T=20$ K. The procedure is the same as in the classical simulation of Ref. 4.

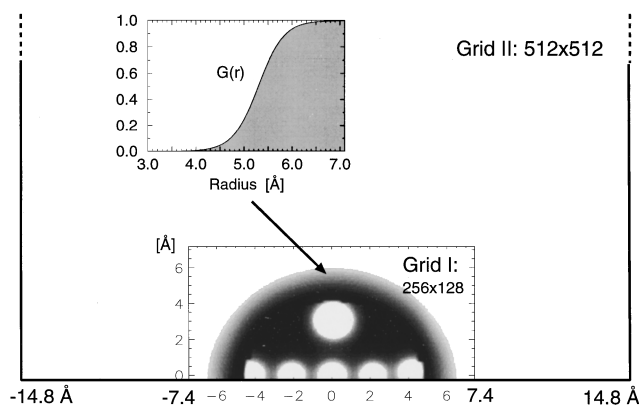


FIG. 2. The two numerical grids used for the quantum propagation. Only a part of the large grid II is shown. The grey scale is a superposition of the potential and the transfer function $G(\mathbf{q})$, which circularly surrounds the region, where hydrogen interacts with the chlorine atom and the surface. The repulsive potentials of the surface ions and the chlorine atom can be seen as white circles. The inset shows the smooth step function $G(\mathbf{q})$.

III. METHODS

A. Quantum propagation on two grids

The wave packet is propagated by the Chebychev method¹⁷ and a fast Fourier transformation scheme for the evaluation of the Hamilton operator. A large numerical grid is needed to represent the wave function occupying a wide region in space after scattering from the surface. The large momentum of the final hydrogen requires a dense spacing of the grid points ($\Delta x = \hbar \pi / p_{\max} \approx 0.06 \text{ \AA}$). Since a momentum analysis of the scattered wave function is performed, we do not follow the common procedure to absorb the outgoing wave function at some boundary in order to reduce the size of the grid. Instead we split the wave packet into two parts,

$$\psi(\mathbf{q}, t) = \psi_{\text{I}}(\mathbf{q}, t) + \psi_{\text{II}}(\mathbf{q}, t) \quad (1)$$

and propagate each of them on a separate grid (Fig. 2). One of the grids has 256×128 points and covers the interaction region near the surface. A second, larger grid with 512×512 points is used for the potential free region further apart from the surface and the chlorine atom. The propagation of the wave function on the second grid is efficiently performed by analytical methods.¹⁸

Although the linearity of the Schrödinger equation allows an arbitrary splitting (1) of the wave function, in practice a smooth connection between the two grids has to be defined. The splitting must not introduce higher momenta in the split wave functions than can be represented by the grids. Then the artificial features introduced by splitting the wave functions cancel in the complete wave function.

Parts of the wave packet $\psi_{\text{I}}(\mathbf{q}, t)$ near the boundaries of the smaller grid are transferred to the second grid in time intervals of 0.6 fs, which is short enough, that the wave packet $\psi_{\text{I}}(\mathbf{q}, t)$ does not reach the boundaries,

$$\begin{aligned} \psi_{\text{I}}(\mathbf{q}) &\rightarrow \psi_{\text{I}}(\mathbf{q})[1 - G(\mathbf{q})], \\ \psi_{\text{II}}(\mathbf{q}) &\rightarrow \psi_{\text{II}}(\mathbf{q}) + \psi_{\text{I}}(\mathbf{q})G(\mathbf{q}). \end{aligned} \quad (2)$$

The transfer function $G(\mathbf{q})$ is zero in the inner part of the first grid and smoothly reaches a value of 1 for coordinates \mathbf{q} further away from it. Here we used a circular shape for this function with center \mathbf{q}_0 lying 1 a.u. under the O^{2-} -ion at which the HCl is adsorbed (Fig. 2)

$$\begin{aligned} G(\mathbf{q}) &= \tilde{G}(|\mathbf{q} - \mathbf{q}_0|), \\ \tilde{G}(r) &= [1 + e^{-\gamma(r - \bar{r})}]^{-1}, \end{aligned} \quad (3)$$

with the parameters $\bar{r} = 11 \text{ a.u.}$ and $\gamma = 2 \text{ a.u.}^{-1}$.

The second grid (in momentum representation) can also be viewed of as a storage area for those parts of the wave packet on the first grid, which are damped off on the boundaries of the smaller grid. Each grid point accumulates the amount of wave function with a corresponding momentum (direction and energy), determined by Fourier transformation of the damped part of the wave packet.

B. Q/C TDSCF propagation

The general concept of the time-dependent self-consistent field approach^{19–22} goes back to Dirac and Frenkel. A multidimensional wave function $\Psi(q_1, q_2, t)$ is approximated by a product of wave functions $\psi_i(q_i, t)$ each with lower dimensionality (for simplicity of notation we assume two one-dimensional wave functions),

$$\psi(q_1, q_2, t) = \psi_1(q_1, t)\psi_2(q_2, t). \quad (4)$$

With the variational principle one finds that the wave functions $\psi_i(q_i, t)$ individually obey Schrödinger-type equations with an additional, time-dependent SCF potential $V_i(q_i, t)$.^{20,21} These potentials are the expectation values of the total potential calculated with the wave function for the other part of the system,

$$V_i(q_i, t) = \langle \psi_j | V_{12}(q_1, q_2) | \psi_j \rangle \quad i \neq j. \quad (5)$$

The time dependence of $V_i(q_i, t)$ thus originates from the time dependence of the wave function $\psi_j(q_j, t)$. The Schrödinger equations for the $\psi_i(q_i, t)$ are formally independent, but have to be solved simultaneously at any time t , since the explicit time dependence of their SCF potentials $V_i(q_i, t)$ is determined by the other equation. In this way energy transfer between the modes q_1 and q_2 is incorporated in the treatment.

If the exact wave function $\Psi(q_1, q_2, t)$ is separable at all times, the TDSCF procedure gives the exact result $\Psi(q_1, q_2, t) = \psi(q_1, q_2, t)$. In other cases the TDSCF wave function $\Psi(q_1, q_2, t)$ is the “best”²⁰ separable approximation to the exact solution. By the product ansatz (4) all correlations between the modes q_1 and q_2 are neglected. Therefore this approximation breaks down whenever correlations become important, as, e.g., when the wave function starts to break up into several parts.²³

The formal independence of the Schrödinger equations for the ψ_i allows the use of different propagators for different modes. This is an important advantage as the use of further specific approximations for the individual modes q_i is possible. In the present case one of the wave packets, say $\psi_2(q_2, t)$, behaves rather classically and we therefore replace

the quantum propagation of q_2 by classical propagation. This is common practice in treating the dynamics of heavy atoms. One of the consequences of any classical treatment is the neglect of quantum phase information as will be discussed in Sec. III C 2. The total system is now described by quantum coordinates $q := q_1$ and classical coordinates $R := q_2$. With the Hamiltonian

$$\hat{H}(q, R) = \hat{H}_q(q) + \hat{H}_R(R) + V_{12}(q, R) \quad (6)$$

and the resulting classical forces $F^{\text{cl}}(R) = -\partial\hat{H}_R/\partial R$ the dynamics is determined by *mixed quantum/classical* TDSCF equations,^{22,24}

$$i\hbar\dot{\psi}(q, t) = [\hat{H}_q + V_q(q, t)]\psi(q, t), \quad (7)$$

$$\dot{p}(t) = F^{\text{cl}}(R) + F_R(R, t), \quad (8)$$

$$\dot{R} = p/m.$$

The Schrödinger Eq. (7) contains an additional TDSCF potential $V_q(q, t)$, and the Hamilton Eqs. (8) include an additional TDSCF force $F_R(R, t)$. These quantities describe the effect of the mean field of the other subsystem in each equation through the coupling potential $V_{12}(q, R)$ and the corresponding forces $F_{12}(q, R)$,

$$F_R(R, t) := \langle \psi(q, t) | F_{12}(q, R) | \psi(q, t) \rangle, \quad (9)$$

$$V_q(q, t) := V_{12}[q, R(t)]. \quad (10)$$

In practice the equations are solved by assuming constant TDSCF potentials (forces) within small time steps Δt , during which the modes are propagated independently. After updating the TDSCF values F_R and V_q , the equations are then solved for the next time step Δt .

Among the several different Q/C TDSCF algorithms we here use the method, in which one classical trajectory is propagated together with one wave packet. At the end an average over several such runs for different classical initial conditions is performed.²⁵ In another scheme one wave packet interacts with the average of a trajectory bundle.²⁴

C. Computational aspects

1. Quantum propagator

For solving the time-dependent Schrödinger equation one has a choice between various methods. Since here a large grid is required, efficiency is an important criterion. This in particular favors methods using a polynomial expansion of the propagator over second-order differencing or the split-operator technique.²⁶ For practical purposes two types of polynomial expansion (or Krylov-space based) algorithms can be distinguished.¹⁷ First there is the large class of the “nonuniform” methods, often referred to as “short-time propagators,” like Newton, residuum, or Lanczos method. Second there is the “uniform” approach which is represented by the Chebychev method and its derivatives.

Although the Chebychev method is usually considered as a “long-time propagator,” the crucial parameter of the propagation is $\Delta E \Delta t / \hbar$ (where Δt is the time interval of a single propagation step and ΔE is the energy interval, which

can be represented on the numerical grid). The larger $\Delta E \Delta t / \hbar$ is, the more favorable the Chebychev method becomes in comparison to the nonuniform propagators. Since here ΔE is large we use this method even for the TDSCF calculations, where the time interval Δt is limited by the time dependence of the effective SCF potentials. This is therefore an example for a problem with a time-dependent Hamiltonian, where the Chebychev propagator is not only applicable but even preferable.

2. Validity of the Q/C TDSCF approach

In this study we want to include *some* specific quantum effects in the model of a system, in which most properties are well represented already on a classical level. Besides the zero-point motion of the initially adsorbed HCl molecule an important quantum effect is the interference pattern in the motion of the hydrogen atom and its consequences on the energy and angular spectra. The modeling of some quantum features has to be seen in contrast to the treatment of systems, where a full quantum description is essential for the dynamics. Approximations, which may not work there at all, can safely be used in the present case.

Since for the classical subsystem, the Q/C TDSCF method yields no quantum phase information, the phase of the total system also remains undefined. Observables depending on this phase, like spectroscopic properties must therefore remain undetermined on this level.²² In particular, the absorption spectrum or the corresponding autocorrelation function of the total wave function are beyond the present Q/C TDSCF approach. We want to make two points regarding this issue. First, the failure in producing the absorption spectrum is not caused by the TDSCF separation, but rather a consequence of the classical approximation for one of the subsystems. A quantum/semiclassical TDSCF approach could provide the relevant phase information.^{22,27} Second, despite of the lack in the description of spectroscopic observables, dynamical properties can be obtained by the Q/C TDSCF approximation.^{22,24} Here we are interested in the dynamics of the hydrogen atom, i.e., its angular distribution, velocity distribution and energy transfer. These properties are known to be accurately represented on the Q/C TDSCF level—at least for short times.^{22,24,25} The (exact) quantum dynamics of the hydrogen motion is modified by interaction with the surface on a very short time scale only, which is a favorable condition for the TDSCF approximation.

3. TDSCF coordinates

The TDSCF formalism neglects all correlations between the different sets of modes of the system. Since the numerical effort to describe these correlations scales exponentially with the number of modes, the gain in numerical efficiency is large. An important aspect of the TDSCF approach is the choice of coordinates. Obviously the success of the approximation depends on a proper choice of modes with minimal correlations between them. Here we separate the coordinates of the hydrogen atom from the coordinates of all other particles and represent the two hydrogen coordinates by a

single, two-dimensional wave function. The different mass and time scales of the chosen subsystems reduce correlations between them. Such a separation was used for other hydrogen containing systems and favorably compared to exact calculations.^{28,29} There is also interesting work on similar systems, where a more drastic TDSCF approximation with a separation of the hydrogen coordinates themselves is used.^{5,23}

The TDSCF approximation obeys energy and momentum conservation in the total system.²² For a control of the numerical convergence with respect to the TDSCF time step Δt , a test of energy conservation alone is not sufficient. If Δt is chosen too large, the transfer of energy between the modes can be too small, even if the total energy is conserved. Therefore the results have to be checked by propagation with a considerably smaller Δt , e.g., for a short time interval during which the interaction between the modes is strong.

4. Computational effort

The computational effort of the simulation techniques depends on several parameters. The computation time for the classical simulation is determined by the number of ions used to describe the MgO cluster. This number was not optimized in this study. For a comparison of the classical and quantum simulations it is important to note that the classical distributions reflect the statistics associated with the trajectories for different initial conditions. The statistical significance is controlled by the number of trajectories, while the quantum simulation is just a single, but considerably slower calculation. Here we use 1500 classical trajectories compared to one wave packet propagation.

The ratio of computation times is 6:1:3 for the classical, quantum (rigid surface), and Q/C TDSCF simulations, respectively. The classical simulation takes the largest time, because in each run of the many trajectories the complete MgO cluster dynamics (which is kept frozen in the quantum case and calculated only once for each Q/C TDSCF run) is calculated. The Q/C TDSCF method is just three times slower than the quantum propagation, although over 1500 additional coordinates of the MgO ions and the chlorine atom are propagated.

IV. RESULTS

A. Resonances and absorption spectrum

The absorption spectrum for the excitation of HCl to its repulsive ¹II state becomes modified when the molecule is adsorbed on a MgO surface. For HCl in the gas phase the broad, continuous absorption band shows no structure. However the quantum calculation of the photodissociation dynamics with rigid surface and chlorine atoms leads to an absorption spectrum with a strong oscillating structure (Fig. 3).

The absorption spectrum is determined by the dipole autocorrelation function of a wave packet³⁰ $\phi(t)$

$$\sigma(E + E_0) \propto \int_{-\infty}^{\infty} e^{iEt/\hbar} \langle \phi(0) | \phi(t) \rangle dt. \quad (11)$$

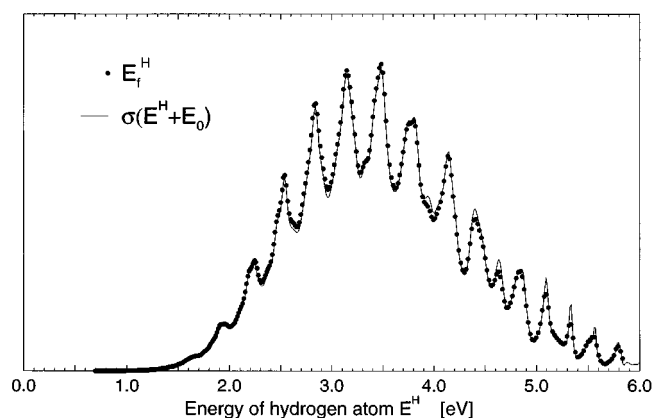


FIG. 3. Absorption spectrum of the HCl adsorbate (solid line, shifted to corresponding excess energies) and energy distribution of the hydrogen atom (dots) for rigid surface and chlorine atom positions (see Fig. 11). The peak structure is caused by trapping resonances of the hydrogen atom between the surface and chlorine atom.

The photon energy $h\nu = E + E_0$ is the sum of the excess energy of the photofragments E and the initial binding energy E_0 . The function ϕ is the product of the dipole transition moment μ_{fi} and a wave function propagated from the initial ground state $\psi(0)$,

$$\phi(t) := \mu_{fi} e^{-i\hat{H}t/\hbar} \psi(0). \quad (12)$$

Here we assume that the dipole transition moment is independent of the H–Cl separation in the range of the initial wave function $\psi(0)$. The advantage of the approach (11) is, that only a small area in real space covering the initial wave function is needed for the calculation of the autocorrelation function. Since the latter is decaying rapidly, the propagation is restricted to short times.

The origin of the additional structure in the absorption spectrum is already clear from an one-dimensional model. If we restrict the hydrogen motion to the surface normal, it feels a *binding* potential between the chlorine and the surface. In this potential the energy of the hydrogen atom is quantized with levels shown in Fig. 4 leading to the corresponding structure in the photoexcitation spectrum. In other words, the hydrogen wave packet interferes with itself, while oscillating between chlorine atom and surface. Depending on energy there is destructive or constructive interference leading to different probabilities of the excitation process. Since the hydrogen motion in real is not just one-dimensional, the hydrogen atom finally leaves the surface area and the levels obtain some finite width (Fig. 3).

The position of these resonances in the absorption spectrum can be used to determine potential parameters of the system. In Fig. 4 a one-dimensional cut through the surface and chlorine potentials used in the simulation is shown. The dashed line is a harmonic potential which is reconstructed from the position of the energy peaks in the absorption spectrum and found to be in good agreement with the original potential.

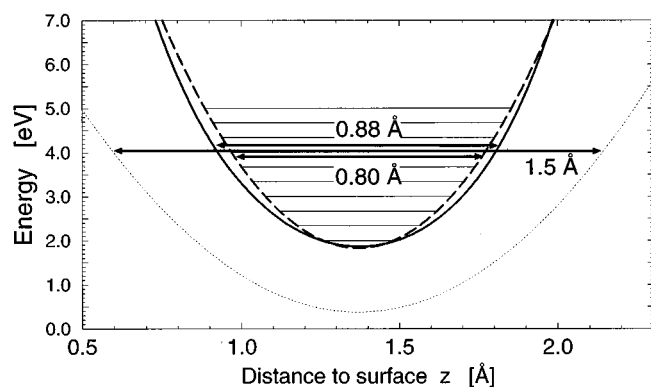


FIG. 4. A harmonic potential (dashed line), reconstructed from the peaks in the absorption spectrum (Fig. 3), and the actual potential used in the simulation (solid line; this is a cut normal to the surface, as indicated in Fig. 1). The energy levels of the harmonic potential correspond to the peaks in the absorption spectrum. The dotted line shows a potential cut (shifted in z -direction to match the minima), assuming a different adsorbate position (Fig. 12) for comparison.

The structure in the absorption spectrum is related to the recurrence peak in the autocorrelation function $\langle \phi(0) | \phi(t) \rangle$ at $t \approx 13$ fs (Fig. 5). The Fourier transformation (11) of this peak is responsible for the oscillating feature in the absorption spectrum. It is caused by that part of the wave packet, which comes back to its initial state $\psi(0)$ after colliding with the surface.

There is another more technical aspect concerning the absorption spectrum. In the approximation of a hydrogen moving in a potential with rigid surface and chlorine atoms, the hydrogen energy is constant. Therefore the final energy distribution coincides with the initial excess energy distribution given by the absorption spectrum. This can be used as a numerical check of the propagation and in particular of the representation on the two distinct numerical grids. The absorption spectrum is calculated on the smaller grid at short times of the propagation, as already mentioned. In contrast, the final energy of the hydrogen is obtained on the second

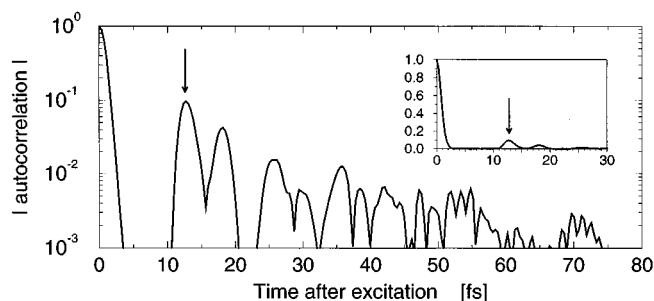


FIG. 5. The modulus of the autocorrelation function $|\langle \psi_H(t) | \psi_H(0) \rangle|$ of the hydrogen wave packet for rigid surface and chlorine atom positions. After a rapid decay of the autocorrelation function, parts of the wave packet are reflected back from the surface to the initial hydrogen state and lead to a first recurrence peak at 13 fs. It is responsible for the oscillating structure in the absorption spectrum.

grid from the asymptotic momentum representation of the wave packet. Both results are shown in Fig. 3 and compare well.

Since the two-dimensional description as well as the approximation of rigid surface and chlorine atom positions overestimates the hydrogen oscillation, we expect the effect to be weaker in reality. The classical treatment of the surface modes does not allow to calculate the absorption spectrum for a nonrigid surface. The related hydrogen energy distribution in this case will be discussed in Sec. IV C.

Although in a classical description the resonances are seen as oscillating trajectories of the hydrogen atom [Fig. 3(d) of Ref. 4], they lead to a quantum effect for the absorption spectrum, which is missing on a classical level. Such correspondence of unstable classical periodic orbits and quantum wave function (“quantum scar”) is discussed in detail in Ref. 31.

B. Angular distribution

The angular distribution of the final hydrogen fragments is shown in Fig. 6. For rigid surface and chlorine atom positions one gets the distributions for monochromatic excitation from the wave function by projection of the corresponding excess energy. Excitation at 193 nm leads to the spectrum in Fig. 6(b). It shows a strong oscillatory interference pattern. Its origin will be discussed in Sec. IV D.

The energy dependent oscillations cancel in the angular spectrum for broad band excitation [Fig. 6(c)], in which an integration over all possible excitation energies is performed. This energy integrated quantum distribution is similar to the classical one [Fig. 6(a)]. Here the spectra for an excitation at 193 nm are shown, but in the classical case the difference for different excitation energies and the distribution for broad band excitation is small. The rainbow peaks at 25° and in particular at 55° are more prominent than in the classical case. The classical scattering shadow, induced by the chlorine atom between $\Theta=0^\circ$ and 20° , can also be seen in the quantum case, although the wave function has a tail into this angular range.

There is a similarity between the quantum and the classical distributions, but the additional effect of interference of the quantum wave function leads to a strong modification of the quantum spectra for monochromatic excitation. These interferences may be overestimated by the assumption of rigid surface and chlorine atom positions. Therefore it is interesting to understand how this effect is influenced by the many additional degrees of freedom in the more realistic model of the surface.

In Fig. 6(d) the motion of the chlorine atom and the MgO ions is described classically within the Q/C TDSCF method, in which inelastic scattering from the surface and energy transfer to the chlorine atom are allowed. There are only slight modifications to the “rigid” angular spectrum [Fig. 6(b)]. After taking into account the thermal motion of the surface by averaging several runs with different initial conditions for the surface ions [Fig. 6(e)], the differences become slightly stronger. The energy integrated angular dis-

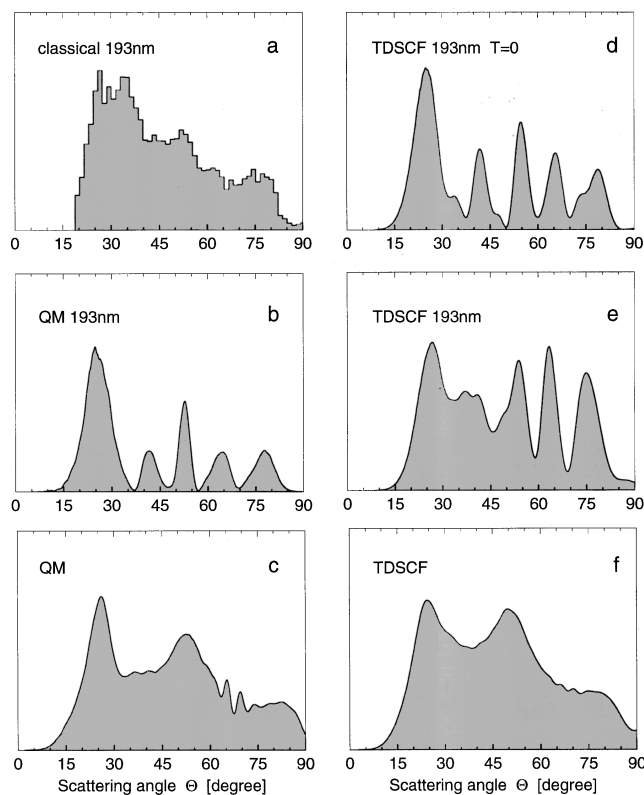


FIG. 6. The angular distribution of the scattered hydrogen atom relative to the surface normal. Quantum wave packet dynamics creates a strong interference structure (b), which is absent in a classical description (a). (a) Classical simulation for a monochromatic excitation at 193 nm. (b) Quantum dynamics with rigid surface and chlorine atom positions; projected to energies corresponding to an excitation at 193 nm (see Fig. 11). (c) Quantum dynamics with rigid surface and chlorine atom positions; energy integrated spectrum (see Fig. 11). (d) Q/C TDSCF simulation for a perfect $T=0$ surface lattice, projected to energies corresponding to excitation at 193 nm. (e) Q/C TDSCF simulation for a surface at $T=20$ K; projected to energies corresponding to excitation at 193 nm (see Fig. 13). (f) Q/C TDSCF simulation; energy integrated spectrum (see Fig. 13).

tribution [Fig. 6(f)] again is similar to its counterpart for rigid surface and chlorine atom positions [Fig. 6(c)].

From the classical study of the system⁴ it has been concluded that the angular distribution is not very sensitive to inelastic effects. This remains true also for the quantum case. As an important consequence, the interference patterns are not destroyed by including the additional degrees of freedom of the surface and the chlorine atom in the more realistic simulation.

C. Energy transfer

The approximation of rigid surface and chlorine atoms implies that the energy distribution of the hydrogen atom is equivalent to the absorption spectrum. When energy transfer through inelastic collisions is considered as in the Q/C TDSCF approach the peaks in the hydrogen energy distribution nearly vanish (Fig. 7). Since we argue that the peaks are already overestimated by our two-dimensional simulation of the hydrogen atom, it is expected that the oscillations completely vanish for the real three-dimensional system.

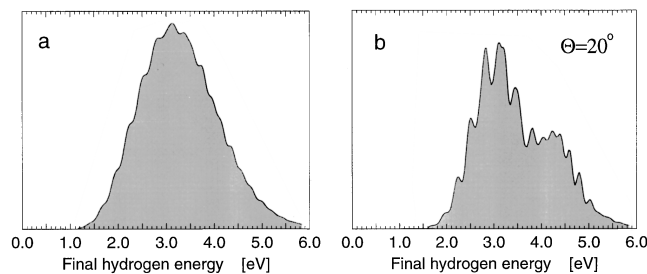


FIG. 7. The energy distribution of the scattered hydrogen atom in Q/C TDSCF description. (a) The energy distribution, integrated over all scattering angles (see Fig. 13). Due to the motion the surface and chlorine atoms the peak structure almost disappears. (b) The energy distribution for a scattering angle of 20° to the surface normal (see Fig. 11). This angular resolved spectrum shows structure even for nonrigid surface and chlorine atoms.

In the angular resolved spectrum, however, the peaks remain clearly distinguishable (Fig. 7) even when inelastic effects are included on the Q/C TDSCF level. Such a more realistic treatment shows the same oscillations as the absorption spectrum in the rigid-surface case.

Experimentally it should even be possible to avoid the averaging due to inelastic scattering by measuring the elastically scattered hydrogen atoms (zero-phonon peak) after monochromatic excitation. In the classical description of the surface modes used here, such an effect due to the quantum nature of phonons is not accounted for.

D. Interference effects in k -space

After the hydrogen atom leaves the surface region and propagates freely, the momentum representation of its wave function no longer changes. This k -space representation of the wave packet is a convenient tool for the analysis of interference effects.^{6,32} Its qualitative form is shown in Fig. 8. The k_x axis is chosen parallel, k_z normal to the surface.

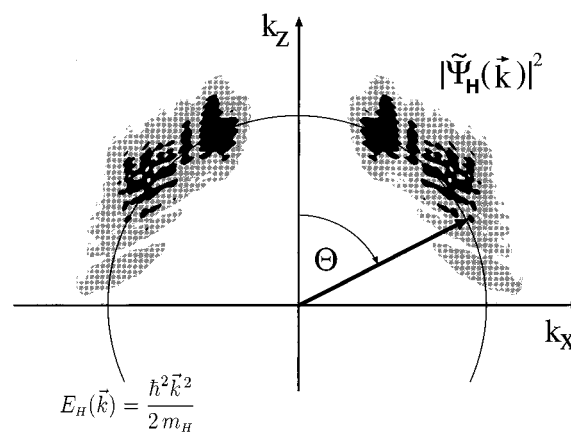


FIG. 8. The hydrogen wave packet $|\tilde{\psi}_H(k_x, k_z)|^2$ in k -space. The distribution of length and direction of the k -vector of the scattered hydrogen defines the energy and angular spectra, respectively. The direction k_x is parallel, k_z is normal to the surface. Due to vanishing of the wave function for negative k_z values and symmetry for positive and negative k_x values, the following detailed views of the wave packets are shown in the first quadrant of the k_x, k_z plane only.

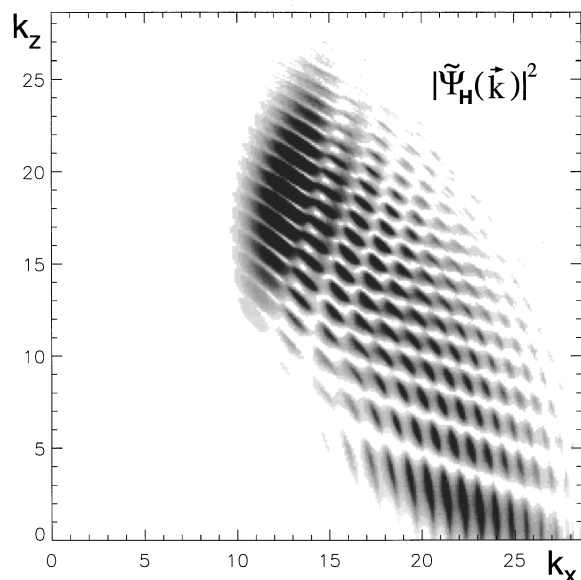


FIG. 9. The hydrogen wave packet $|\tilde{\psi}_H(k_x, k_z)|^2$ after scattering from a flat, rigid surface. The grey scale corresponds to the intensity, k_x and k_z are in atomic units. A strong, regular interference structure can be seen.

Angular resolved energy spectra and energy resolved angular distributions are cuts along lines of constant angle or constant energy (circles). This correspondence to the differential spectra makes the k -space wave packet distribution also an experimentally accessible observable.

1. Interference effect for the flat surface

For an identification of the interference patterns we first investigate a simplified model with a flat, rigid surface. Corrugation is neglected by using only the z dependence of the H-O²⁻-potential. The resulting wave function is shown in Fig. 9. The shape of the wave packet is roughly a circular band around the origin with radii given by the maximal and minimal momenta (corresponding to the possible excess energies) of the hydrogen atom. In directions normal to the surface the band is suppressed due to the chlorine shadow.

The wave packet shows a very pronounced, regular interference pattern. These peaks are responsible for the oscillating structures in the energy resolved angular spectra, as well as in the energy or absorption spectra. The oscillating structure can be explained semiclassically by interference of different trajectories of the hydrogen atom, scattered into the same direction Θ . Depending on their relative phase for a particular energy and direction, they interfere destructively or constructively. A schematic view of two trajectories with the same direction is given in Fig. 10. The interference of these trajectories lead to a pattern in k -space, where the maxima come to lie approximately on circles of constant momenta. This circular structure can clearly be identified in Fig. 9 and originates from the fact, that qualitatively the trajectories differ just by an additional oscillation of the hydrogen between the chlorine atom and the surface (Fig. 10). The corresponding phase difference is (roughly) independent of the scattering angle Θ . Therefore one gets circles in

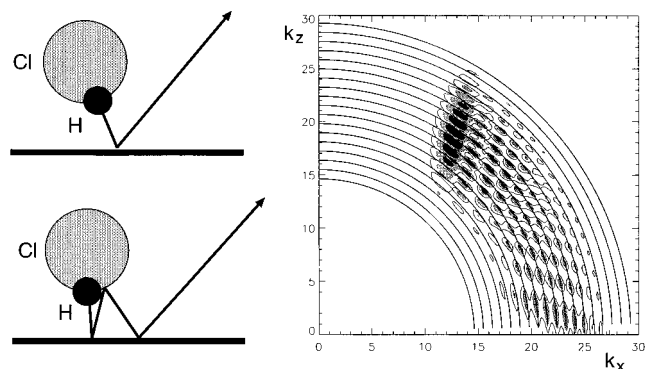


FIG. 10. The structure in the wave packet in Fig. 9 for a flat surface originates (from a semiclassical point of view) from hydrogen trajectories, which scatter into the same direction and interfere in the detector. As an example schematic views of two types of trajectories are shown. Their interference leads to a circular pattern in k -space, which is shown together with the wave packet of Fig. 9.

k -space and their distance is given by 2π increments of the phase shift on this path of the hydrogen atom. As a matter of fact, this is just a different view of the origin of the interference peaks in the absorption spectrum discussed in Sec. IV A.

2. Interference effect for the corrugated surface

Comparison of Fig. 9 with the result for the corrugated, rigid surface (Fig. 11) shows the influence of surface corrugation on the wave function in k -space. The scattering shadow at normal angles Θ now becomes smaller. Directions with smaller Θ are reached also by hydrogen atoms which

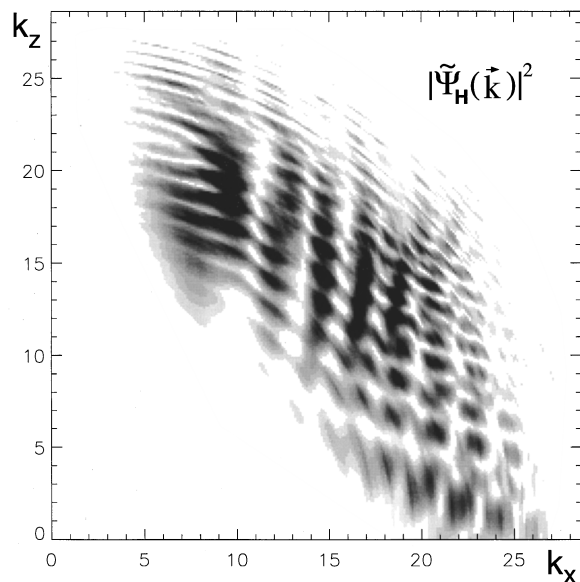


FIG. 11. The hydrogen wave packet $|\tilde{\psi}_H(k_x, k_z)|^2$ after scattering from a corrugated, rigid surface. Comparison with Fig. 9 shows the influence of surface corrugation on the k -space pattern. More quantitative information on the interference structure can be found in the corresponding energy (Fig. 3) and angular [Figs. 6(b), 6(c)] spectra.

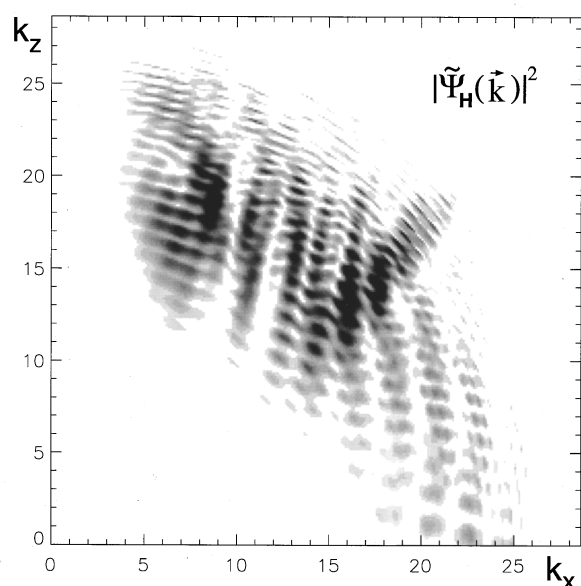


FIG. 12. The hydrogen wave packet $|\tilde{\psi}_H(k_x, k_z)|^2$ as in Fig. 11, but for an adsorbate located 0.6 Å further apart from the surface. Compare Fig. 4 for the strong influence of adsorbate geometry and potential on the interference pattern.

are reflected from surface areas further away from the chlorine atom [compare the trajectory in Fig. 3(b) of Ref. 4].

In directions around $\Theta \approx 50^\circ$ the intensities are higher and here also the classical dynamics simulation shows a rain-bow peak caused by surface corrugation.

Although the interference pattern is not as regular as in the flat surface case, the similarity can clearly be seen. Therefore we interpret the main structure by the same mechanism as for the flat surface. Surface corrugation leads to a slight distortion, rather than being the main mechanism of its origin. Nevertheless corrugation induces significant change in the momentum distribution.

An example for the effect of initial adsorbate geometry is shown in Fig. 12. Here HCl was assumed to be located 0.6 Å further away from the surface. The larger distance is reflected in faster oscillations of the interference pattern in k -space.

3. Interference effect and inelastic collisions

Figure 13 shows the hydrogen wave packet when the classical motions of the chlorine atom and MgO ions are treated on the Q/C TDSCF level. Then inelastic collisions of the hydrogen atom with the surface and the chlorine atom and the thermal motion of the surface are included in the dynamical description.

The hydrogen atom is scattered from surface ions now having variable positions due to their thermal motion. Therefore hydrogen atoms (or parts of the wave packet) which are released initially into the same direction may become reflected into different directions. Moreover the energy distribution of the hydrogen atom is affected by energy transfer to the MgO crystal and the chlorine atom. Both mechanisms broaden the wave packet peaks and wash out most of the

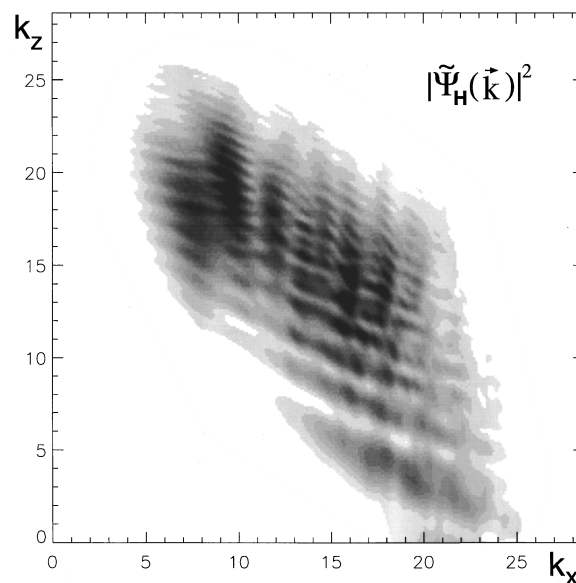


FIG. 13. The hydrogen wave packet $|\tilde{\psi}_H(k_x, k_z)|^2$ after scattering from the MgO surface. The motions of the chlorine atom and the crystal ions are described in Q/C TDSCF approximation. Although the interference pattern is mostly washed out by the additional degrees of freedom, most of the peaks remain clearly distinguishable [compare Figs. 6(e) and 7].

structure in the interference pattern. Nevertheless the peaks remain distinguishable and therefore can be used to extract information on adsorbate geometry and surface potential.

V. SUMMARY AND DISCUSSION

We investigate the photodissociation dynamics of HCl/MgO on different levels of approximation; classical,⁴ quantum mechanical with a restricted number of degrees of freedom, and in a mixed quantum/classical TDSCF framework. The classical description (with zero-point energy of the adsorbate included) shows most of the general aspects of the dynamics and gives an intuitive picture of the processes in the system. For the quantum wave packet dynamics of the hydrogen atom the surface and chlorine degrees of freedom have to be frozen. The most prominent modification of the classical results is the interference pattern in the angular distribution and a pronounced structure in the absorption spectrum.

From the classical simulation it is known that there is considerable energy loss of the hydrogen atom during its collisions with the surface (about 15%) and the chlorine atom (about 5%). Within the Q/C TDSCF approximation the quantum interference can be described together with these inelastic collisions and the thermal motion of the surface. The angular distribution of the hydrogen atom is not changed considerably when the assumption of a rigid surface is released. This is an interesting result by itself. On the other hand, the peak structure in the energy distribution averaged over all final angles practically disappears in the Q/C TDSCF case. But the structure can still be seen in the angular resolved spectra, and the energy distribution for given final

angle is actually a property easier to measure in an experiment.

The interference effect in the angular distribution and the resonance structure in the absorption spectrum are caused by the temporary trapping of the hydrogen atom between the surface and the chlorine atom. This is the same effect as found before in the photodissociation of HCl in an Ar \cdots HCl complex.^{25,28,33} The intensity of the effect depends on the probability for hydrogen to become backscattered to the chlorine atom. For the rare gas complex this probability is lower, because most of the hydrogen will miss the argon atom due to the zero-point motion of the HCl molecule. Here, however, the hydrogen atom hits the MgO surface and then scatters back. The surface corrugation directs also some hydrogen back to the chlorine, which is not reflected from the surface region directly beneath the chlorine atom. Nevertheless even for the Ar \cdots HCl complex the interference can be seen,²⁷ at least if the width of the initial wave packet is reduced in the simulation.^{28,33} This is particularly interesting since for the axially-symmetric Ar \cdots HCl problem it is possible to consider all three spatial coordinates, thus avoiding the overestimation of the effect in a two-dimensional framework. In the case of HCl/MgO we expect a stronger binding, i.e., a narrower wave packet, and an amplification of the effect. Therefore the resonances should exist even if the hydrogen motion is not restricted to two dimensions, and there are good chances for observation in a realistic experiment. Pump-probe spectroscopy is an alternative approach to observe the resonance effect experimentally, even when the corresponding structure in the absorption spectrum and the hydrogen energy distribution are weak.

The possibility to measure the interference pattern in the hydrogen distributions is important, because it contains much of the information on the potential surface and the geometry of the adsorbate. We found good agreement between the potential on the chlorine-surface axis and a potential reconstructed from the resonance pattern in the hydrogen energy distribution.

It was also shown that the fundamental pattern of the interference can be seen with a flat surface. Surface corrugation leads to a significant modification of this pattern. Therefore information on corrugation of the potential can in principle be obtained from double differential measurements (energy and angle), even if the interpretation of such data are not as straightforward as, e.g., the interference for scattering from a regular grid.

We expect that these results are qualitatively valid for any HX adsorbate dissociation on an ionic insulator surface, as long as the HX is oriented along the surface normal with the hydrogen pointing to the ionic crystal. For example the

HF/LiF system is reported to have such a geometry.⁶ This allows some flexibility for the design of an experimental setup to measure the interference patterns in practice. With high resolution, angular resolved energy measurements of the hydrogen atom at different excitation wavelengths it should be possible to resolve the oscillations in the spectra.

ACKNOWLEDGMENTS

We are grateful to M. R. Chacon-Taylor and M. McCarthy for providing geometrical information on the HCl/MgO adsorbate system prior to publication. The Fritz Haber Research Center is supported by the Minerva Gesellschaft für die Forschung GmbH, München, Germany.

- ¹M. I. McCarthy and R. B. Gerber, *J. Chem. Phys.* **93**, 887 (1990).
- ²J. V. Setzler, Z. H. Huang, and H. Guo, *J. Chem. Phys.* **103**, 4300 (1995).
- ³V. J. Barclay, W. H. Hung, J. C. Polanyi, G. Zhang, and Y. Zeiri, *Faraday Discuss.* **96**, 129 (1993).
- ⁴M. Hintenender, F. Rebentrost, R. Gerber, and R. Kosloff, *J. Chem. Phys.* **102**, 578 (1995).
- ⁵J. Y. Fang and H. Guo, *Chem. Phys. Lett.* **235**, 341 (1995).
- ⁶V. J. Barclay, J. C. Polanyi, Y. Zeiri, and R. Kosloff, *J. Chem. Phys.* **98**, 9185 (1993).
- ⁷T. Seidemann and H. Guo, *J. Chem. Phys.* **103**, 2745 (1995).
- ⁸B. Jackson, *J. Chem. Phys.* **90**, 140 (1989).
- ⁹M. Messina and R. D. Coalson, *J. Chem. Phys.* **95**, 8977 (1991).
- ¹⁰G. D. Billing, Quantum-classical methods, in *Numerical Grid Methods and Their Application to Schrödinger's Equation*, edited by C. Cerjan (Kluwer Academic, New York, 1993), pp. 121–139.
- ¹¹L. Liu and H. Guo, *Chem. Phys. Lett.* **237**, 299 (1995).
- ¹²R. B. Gerber and R. Alimi, *Chem. Phys. Lett.* **173**, 393 (1990).
- ¹³M. R. Chacon-Taylor and M. I. McCarthy, *J. Phys. Chem.* **100**, 7610 (1996).
- ¹⁴R. Kosloff and Y. Zeiri, *J. Chem. Phys.* **97**, 1719 (1992).
- ¹⁵M. I. McCarthy, R. B. Gerber, K. A. Trentelman, P. Strupp, D. H. Fairbrother, P. C. Stair, and E. Weitz, *J. Chem. Phys.* **97**, 5166 (1992).
- ¹⁶M. H. Alexander, B. Pouilly, and T. Duhoo, *J. Chem. Phys.* **99**, 1752 (1993).
- ¹⁷R. Kosloff, *Annu. Rev. Phys. Chem.* **45**, 145 (1994).
- ¹⁸R. Heather, *J. Chem. Phys.* **86**, 5009 (1987).
- ¹⁹P. A. M. Dirac, *Proc. Cambridge Philos. Soc.* **26**, 376 (1930).
- ²⁰A. D. McLachlan, *Mol. Phys.* **8**, 39 (1964).
- ²¹E. J. Heller, *J. Chem. Phys.* **64**, 63 (1976).
- ²²R. B. Gerber, V. Buch, and M. A. Ratner, *J. Chem. Phys.* **77**, 3022 (1982).
- ²³J. Y. Fan and H. Guo, *J. Chem. Phys.* **101**, 5831 (1994).
- ²⁴R. Alimi, R. B. Gerber, A. D. Hammerich, R. Kosloff, and M. A. Ratner, *J. Chem. Phys.* **93**, 6484 (1990).
- ²⁵A. Garcia-Vela, R. B. Gerber, and D. G. Imre, *J. Chem. Phys.* **97**, 7242 (1992).
- ²⁶C. Leforestier *et al.*, *J. Comp. Phys.* **94**, 59 (1991).
- ²⁷A. Garcia-Vela and R. B. Gerber, *J. Chem. Phys.* **98**, 427 (1993).
- ²⁸A. Garcia-Vela and R. B. Gerber, *J. Chem. Phys.* **103**, 3463 (1995).
- ²⁹A. B. McCoy, R. B. Gerber, and M. A. Ratner, *J. Chem. Phys.* **101**, 1975 (1994).
- ³⁰E. J. Heller, *J. Chem. Phys.* **68**, 2066 (1978).
- ³¹E. J. Heller, *Phys. Rev. Lett.* **53**, 1515 (1984).
- ³²R. Kosloff, *J. Phys. Chem.* **92**, 2087 (1988).
- ³³T. Schröder, R. Schinke, M. Mandziuk, and Z. Bačić, *J. Chem. Phys.* **100**, 7239 (1994).